# Technical report: Antiproton-proton annihilation at rest into $K_L K_S \pi^0 \pi^0$

Kersten Braune and Christian Felix Ludwig-Maximilians-Universität München

April 29, 1996

# 1 Introduction

This is the first study of the  $K_LK_S\pi^0\pi^0$  final state produced in  $\bar{p}p$  annihilation at rest. The primary objective is to search for resonances in the various two- and three-body intermediate states. These include resonances decaying to  $(\phi\pi^0)$ ,  $(K^*K)$ ,  $(K\bar{K}\pi^0)$  or  $(K\pi^0\pi^0)$ . The  $K\bar{K}\pi$  sub-system has been studied extensively since 30 years and has revealed the presence of several resonances in the  $1400\,\mathrm{MeV/c^2}$  mass region. It has mostly been studied in its  $K_SK^\pm\pi^\mp$  form, which can have positive or negative charge parity  $C=\pm 1$ . In most previous analyses,  $K\bar{K}\pi$  seems to be dominated by C=+1 states. In radiative  $J/\psi$  decays or  $\gamma\gamma$  interactions it can only be produced with C=+1 anyway. In the present study, the  $K\bar{K}\pi$  system is observed as  $K_LK_S\pi^0$  and therefore exhibits pure C=-1 symmetry. This clean environment allows further investigation of possible  $0^{--}$  and  $1^{--}$  states [1] outside the quark model or of the little known strangeonium of the  $1^{+-}$  nonet [2].

In this analysis, the reaction  $\bar{p}p \rightarrow K_L K_S \pi^0 \pi^0$  is observed in the all-neutral final state with 8 photons and missing energy. The  $K_L$ -meson has a lifetime of  $\tau = 55.2 \times 10^{-8}$ s and a mean momentum of 330 MeV/c, corresponding to a mean flight path of 10m before it's decay. Therefore, the  $K_L$  will most likely decay outside the detector and can be identified by missing energy and momentum in an otherwise complete event. This method is spoiled, if the  $K_L$  interacts strongly in the material of the detector, producing charged tracks in the JDC and/or energy deposits in the crystals. No effort is made to recuperate events with  $K_L$  interactions or decay, even though the data sample could in principle be doubled by taking them into account. A similar loss in statistics (this time a factor of 3) is introduced by accepting only the two- $\pi^0$  decay of the  $K_S$ -meson. These losses have to be seen in relation to the quality of data and little background in the chosen all-neutral channel, which make them acceptable. Finally, it should be mentioned, that only the two- $\gamma$  decay mode of the  $\pi^0$  is considered.

# 2 Data Selection

The  $K_LK_S\pi^0\pi^0$  final state was selected from the all-neutral data taken in nine run periods from December 1989 up to October 1991 which resulted, after reconstruction, in  $17\times10^6$  events on tapes. In addition, data from a special missing energy trigger run (total energy in the barrel was required to be less than  $1600\,\mathrm{MeV}$ ) in June'91 were also used, which amounted to  $0.37\times10^6$  reconstructed events on tapes. The numbers of reconstructed events are given Table 1, separately for each run period. The total numbers of events correspond to  $425\times10^6$  resp.  $58\times10^6$  pp annihilations, where trigger-enrichment factors of 25, resp.  $25\times6.2$  have been used.

## 2.1 Missing Energy 8 PED Events

The first step in the analysis is the selection of 8-PED events with missing energy, corresponding to 8 photons from the decay of 4  $\pi^0$ s and the  $K_L$ -meson, which leaves the detector without interaction. Only three cuts have to be applied for a clean selection of these events out of the all-neutral data sample of  $17\times10^6$  events:

- 1. Rejection of events with charged tracks in the JDC, coming mainly from  $\gamma$ -conversions, backsplash from the barrel and  $K_S$  decays into  $\pi^+\pi^-$  outside the PWCs. This reduces the total number of events  $16\times10^6$ .
- 2. Requirement of exactly 8 PEDs above 20 MeV in the crystals leaves  $1.5 \times 10^6$  events.
- 3. The total energy in the crystals must be in the range 970...1450 MeV corresponding to the kinematically allowed region and detector resolution for a non-interacting  $K_L$  from the reaction  $\bar{p}p \rightarrow K_L K_S \pi^0 \pi^0$ . The  $K_L$  momentum is between 0 and  $686 \, \text{MeV/c}$ , leading to a total energy deposit of the accompanying 8 photons from 1030 up to  $1378 \, \text{MeV}$  in the crystals. This cut reduces the accepted events to  $0.18 \times 10^6$ , the final sample of missing-energy-8-PED-events.

The accurate numbers of left-over events after the above cuts are given for each run period in Table 2.

# 2.2 Missing Energy 8 Gamma Events

The next step in the selection procedure is the interpretation of the missing-energy-8-PED-events as K<sub>L</sub>-8-photon-events. This requires further cuts, one on the direction of PEDs and one on the direction of missing momentum. The containment of the whole photon shower in the crystals can only be guaranteed,

if the PED is not in crystal type 13. Events with such PEDs are therefore removed, leaving  $12\times10^4$  events.

Missing energy in the crystals can come about in many ways; inefficiencies and limited solid angle coverage. In the crystal barrel detector only the latter is of importance and must be taken into account. Charged particles or photons can escape through the forward and backward holes, giving a  $K_L$  signature of missing energy. This can be seen in Fig. 1a, which shows the missing momentum as a function of the polar angle  $\cos\theta$ . The escaping particles can be clearly seen near  $\cos\theta=\pm 1$  and also near  $\theta=90^\circ$ , where the two barrel halves join together. On the other hand, the coverage is azimuth angle  $\Theta$  is uniform and complete (Fig. 1b). Events with missing momentum pointing in the direction of the forward/backward holes are removed, in other words, only events with a missing momentum at polar angles  $21^\circ < \theta < 159^\circ$  are kept for further analysis, in this case about  $97\times10^3$ .

These cuts result in a clean definition for PEDs which can now be interpreted as photons. The PED energy distribution is shown in Fig. 2 and has the expected behaviour without any signs from electromagnetic split-offs, which would appear as a spike at the low energy cutoff. It was therefore not necessary to use any of the standard crystal barrel split-off recognition programs. The influence of these cuts, detailed for each run period are given in Table 3.

### 2.2.1 Missing Energy 4 $\pi^0$ Events

A data sample consisting of nearly  $\times 10^5$  events with a clean definition of missing energy/momentum and of eight photons has been prepared. The overall  $\pi^0$  signal is shown in the invariant  $\gamma\gamma$  mass spectrum in Fig. 3. A narrow  $\pi^0$  peak sits on top of a large combinatorial background and there is no hint for an  $\eta$  signal. This non-appearance of the  $\eta$  is due to the small phase space for the reaction  $\bar{p}p \rightarrow K_L K_S \pi^0 \eta$ .

An extended view of the  $\pi^0$  peak is also shown in Fig. 3. The peak is clearly asymmetric and can be fitted by a Gaussian with width  $\sigma_1$  for masses lower than the mean and width  $\sigma_2$  for masses above the mean. The asymmetry is due to  $\pi^0$ s from  $K_S$  decay which do not come from the vertex in the centre of the detector. Therefore the momentum of photons from  $K_S$  decay  $\pi^0$ s is measured too low, although their energy is properly measured and finally, the mass of the  $\pi^0$  comes out lower than the nominal value. This can be reproduced well using the CB- $\pi^0$ -finder, where the highest efficiency is reached when the  $\pi^0$ -mass is reduced to  $m_{\pi^0}=131 \,\mathrm{MeV/c^2}$ . In about a quarter of all events the  $\pi^0$ -finder finds four  $\pi^0$ s.

The 2-dimensional energy versus momentum spectrum for these missing-energy- $4-\pi^0$ -events is shown in Fig. 4a. A strong band, representing  $K_L$ -mesons, dominates the spectrum. The  $K_L$  can also be seen nearly free of background in the  $4\pi^0$ -missing-mass plot in Fig. 4b. A gaussian fit with quadratic background gives a mass of  $m_{K_L} = 510 \,\mathrm{MeV/c^2}$  and width of  $\sigma = 41 \,\mathrm{MeV/c^2}$  for the  $K_L$  signal.

The effect of a cut on the one-dimensional missing mass spectrum onto the two-dimensional energy versus momentum spectrum can be seen in Fig. 4c. Only events outside the  $K_L$  window of 400 to 600 MeV/c² are plotted and the cut follows well the curved  $K_L$  band. For events belonging to this band the invariant  $\pi^0\pi^0$  mass is shown in Fig. 4d. A nice, slightly asymmetric  $K_S$  signal, sits on a combinatorial (not only though) background. It has a mass of  $m_{K_S}$ =491 MeV/c² and width of  $\sigma$ =35 MeV/c². As expected, the  $K_S$  mass lies below the PDG mass (about 6 MeV/c²), a result of the already mentioned wrong momentum measurement of photons coming from  $\pi^0$ s coming from the  $K_S$ , which do not decay at the primary reaction vertex.

Before the events are kinematically fitted, they are subjected to a cut on the missing mass with respect to the 4  $\pi^0$ . Only events in the  $K_L$ -window between 400 and  $600 \, \mathrm{MeV/c^2}$  are accepted, which results in the final preselection sample of  $44 \times 10^3$  events. Table 4 gives the detailed numbers per run period.

#### 2.3 Kinematic Fits

The 44608 preselected events of the type missing energy in K<sub>L</sub> window and 8 photons are kinematically fitted with the following three hypotheses:

1. 
$$\bar{p}p \rightarrow K_L^{missing} 8\gamma$$
 (1C)

$$2.~\bar{p}p{\to}K_L^{missing}K_S\pi^0\pi^0,~K_S{\to}\pi^0\pi^0,~4\pi^0{\to}8\gamma~(6C)$$

3. 
$$\bar{p}p \rightarrow K_L^{missing} 3\pi^0 \eta$$
,  $3\pi^0 \rightarrow 6\gamma$ ,  $\eta \rightarrow 2\gamma$  (5C)

4. 
$$\bar{p}p \rightarrow \phi \pi^0 \pi^0$$
,  $\phi \rightarrow K_L^{missing} K_S$ ,  $K_S \rightarrow \pi^0 \pi^0$ ,  $4\pi^0 \rightarrow 8\gamma$  (7C)

The events have to pass hypotheses (1) and (2) but not (3). There exists only one possible combination for the first hypothesis and 37,230 events pass it with a confidence level above 1%. The second hypothesis can be realized in 630 different ways and for the third hypothesis there are 420 possible combinations. It is not astonishing that more than one combination has a confidence level above 1%. In fact, as shown in Fig. 5, for about 50% of the events the kinematic fitting package finds more than one good combination. In this case, the combination with the highest confidence level is chosen for further analysis. The confidence level distribution for hypothesis 2 becomes flat above 10% (Fig. 5), which was chosen as cut for the final event selection. In addition the confidence level for the third hypothesis had to be smaller than 1%. The final sample of  $K_L K_S \pi^0 \pi^0$  events consists of 7,434 events which were used in the partial-wave-analysis. Table 5 summarizes the kinematic fit statistics and the pulls are shown in Fig. 5.

## 2.4 The Final Data Sample

The quality of the final event sample is indicated in the distributions of the measured (not kinematically fitted) energies and momenta of the eight photons (Fig. 6). When photons were combined to  $\pi^0$ s, the kinematic fit solution was taken. The invariant  $\gamma\gamma$  mass shows a narrower  $\pi^0$  peak as compared to Fig. 3 but the signal is still slightly asymmetric, which is a sign that the kinematic fit has removed some events with a high  $K_S$  momentum. This must be a small effect, since the invariant  $\pi^0\pi^0$  mass spectrum shows a symmetric  $K_S$  peak with a mass of  $492\,\mathrm{MeV/c^2}$ , still  $7\,\mathrm{MeV/c^2}$  lower than the nominal PDG value. The background below the  $K_S$  peak is of purely combinatorial nature. A Gaussian fit to this peak gives  $7,540\pm190$  events with a  $K_S$ , close to the expected number of 7,434. The (already) small background below the missing mass  $K_L$  peak has completely disappeared.

The above discussion has shown, that the final sample of  $K_LK_S\pi^0\pi^0$  events is very clean. The only remaining problem might be photons which were wrongly combined to  $\pi^0$ 's and  $\pi^0$ 's which were wrongly combined to  $K_S$ 's. The number of wrongly combined  $\pi^0$ 's can be estimated by plotting the invariant  $\gamma\gamma$  mass for all combinations which were rejected by the kinematic fit. This leads to 24 entries per event and is shown in Fig 7a. There is no sign for wrongly combined  $\pi^0$ 's.

The situation is not as clean for the combination of  $\pi^0$ 's to a  $K_S$ , shown in Fig 7b. In this case there are 5 entries per event and the spike-dip structure is due to wrongly combined  $\pi^0$ 's to a  $K_S$ . Their number was estimated to  $760 \pm 57$  above and  $520 \pm 23$  below the smooth curve through the data points. Such a wrong  $K_S$  event contributes twice to the  $\pi^0\pi^0$  mass spectrum which gives a background of wrong  $K_S$  combinations of  $10 \pm 1\%$ .

The momentum distributions of  $K_L$  and  $K_S$  mesons should be identical since they are presumably produced by strong interactions. Their momentum spectra and the  $K_S\pi^0$  and  $K_L\pi^0$  invariant masses are superimposed in Fig 8. The spectra are fairly consistent, but slight, systematic differences can be seen. The  $K_S$  momentum spectrum is shifted to lower momenta, as expected from the wrongly assumed decay vertex in the centre of the detector. Furthermore, the interaction probability of low energy  $K_L$  mesons in the crystals is higher than for high energy  $K_L$  and more of those low energy ones are rejected by the requirement of missing energy, i.e. non-interacting  $K_L$  mesons.

The K\* spectra also show a slight systematic difference in the mass region between 700 and  $800 \, \text{MeV/c}^2$ . Here the  $K_S \pi^0$  invariant mass has something like a small peak. This enhancement seems to be produced from wrongly combined  $K_S$  since both K\* spectra look alike, if they are plotted for invariant  $\pi^0 \pi^0$  masses outside the mass range of 450 to  $500 \, \text{MeV/c}^2$ , where the wrongly combined  $K_S$  come from.

In conclusion, the final data sample of 7,434 kinematically fitted  $K_SK_L\pi^0\pi^0$  events is free from background events, but contains 10%  $K_S$  mesons combined

from the wrong pions.

run period		all-neutral
		${ m events}$
December	1989	$1,\!258,\!297$
June	1990	$1,\!495,\!498$
July	1990	$3,\!565,\!702$
September	1990	$1,\!313,\!379$
November	1990	$4,\!535,\!953$
May	1991	$1,\!574,\!809$
June	1991	$1,\!471,\!622$
June ( $E_{miss}$ trigger)	1991	375,720
August	1991	$1,\!685,\!878$
October	1991	$93,\!066$
Sum		17,369,924

Table 1: Number of all-neutral events on DSTs for each run period used in the  $K_L K_S \pi^0 \pi^0$  analysis.

run period		no charged	8 PEDs	total
		${ m tracks}$	$> 20\mathrm{MeV}$	energy
December	1989	$1,\!195,\!439$	$85,\!525$	11,632
June	1990	$1,\!342,\!961$	$138,\!319$	11,747
July	1990	$3,\!214,\!822$	$250,\!427$	$25,\!635$
September	1990	$1,\!146,\!405$	$119,\!869$	$13,\!610$
November	1990	$4,\!112,\!264$	$440,\!351$	44,728
May	1991	$1,\!354,\!511$	$139,\!616$	13,787
June	1991	$1,\!318,\!353$	$140,\!454$	15,036
June ( $E_{miss}$ trigger)	1991	$353,\!576$	$38,\!334$	$21,\!294$
August	1991	$1,\!485,\!522$	$159,\!998$	17,924
October	1991	$80,\!532$	8,724	898
Sum		15,604,385	$1,\!521,\!617$	176,291

Table 2: Number of remaining events after charged tracks, eight gamma and missing energy cuts.

run period		type 13	$cos  heta_{ec{p}_{miss}}$
Dec./June	89/90	13,873	10,972
July	1990	$18,\!441$	$15,\!259$
September	1990	9,448	7,337
November	1990	$32,\!793$	$25,\!635$
m May/June	1991	$20,\!694$	15,892
June ( $E_{miss}$ trigger)	1991	$15,\!029$	$11,\!622$
Aug/Oct.	1991	$12,\!621$	9,842
Sum		122,899	$96,\!559$

Table 3: Number of events after cuts on PEDs in crystal type 13 and direction of missing momentum.

run period		$ m K_L$
		window
Dec./June	89/90	4,958
July	1990	6,585
September	1990	$3,\!326$
November	1990	$12,\!146$
m May/June	1991	7,741
June $(E_{miss} \text{ trigger})$	1991	5,418
Aug/Oct.	1991	4,434
Sum		44,608

Table 4: Number of events in the final preselection sample after the cut on missing mass, selecting  $K_L$  events, for each run period.

hypothesis and confidence level cut	events
$\mathrm{CL}(\mathrm{K_L}8\gamma) > 1\%$	37,230
$\mathrm{CL}(\mathrm{K_L}\mathrm{K_S}\pi^0\pi^0)>1\%$	$11,\!542$
$  \ \mathrm{CL}(\mathrm{K_L} \mathrm{K_S} \pi^0 \pi^0) > 1\% \ \ \mathrm{and} \ \ \mathrm{CL}(\mathrm{K_L} \mathrm{K_S} \pi^0 \eta) < 1\%$	10,815
$ \; { m CL}({ m K_L}{ m K_S}\pi^0\pi^0)> 10\% \; { m and} \; { m CL}({ m K_L}{ m K_S}\pi^0\eta)< 1\% \;  \;$	$7,\!434$
$\mathrm{CL}(\phi\pi^0\pi^0) > 1\%$	1546

Table 5: Number of events after confidence level cuts.

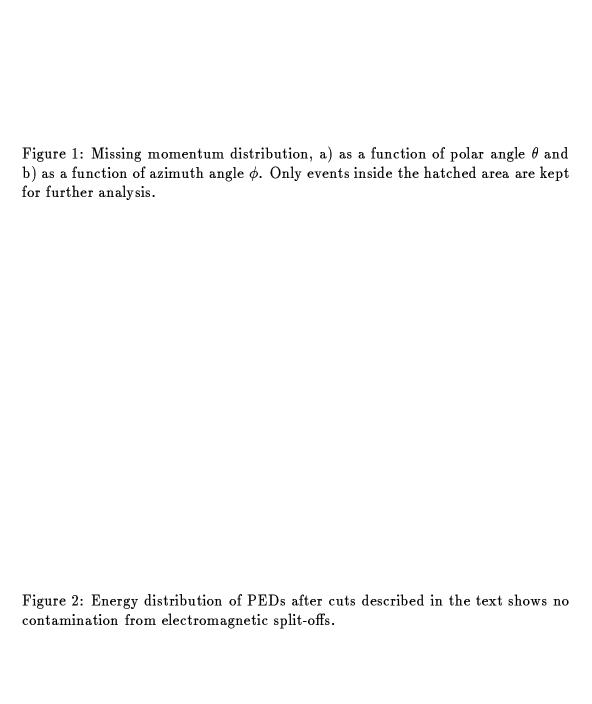
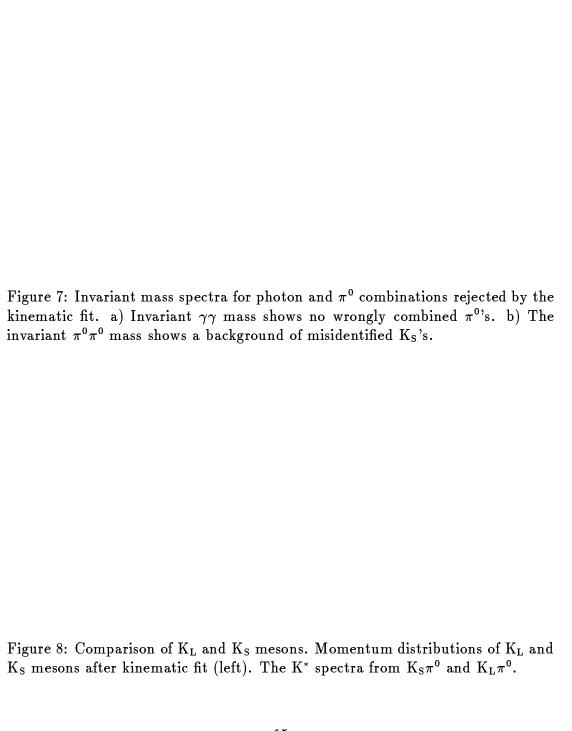


Figure 3: Invariant  $\gamma\gamma$  mass distribution for all possible 28 combinations. The inlay shows a window around the  $\pi^0$  peak with superimposed fit.

Figure 4: Missing-energy-4- $\pi^0$ -events; a) the total energy versus momentum spectrum shows a strong  $K_L$  band; b) the missing mass spectrum shows a strong  $K_L$  peak; c) total energy versus momentum spectrum with  $K_L$  cut on missing mass spectrum; d) invariant  $\pi^0\pi^0$  spectrum after  $K_L$  cut shows clean  $K_S$  peak.

Figure 5: Kinematic fit quality plots. The number of good combinations for hypothesis 2 with confidence level above 1% (upper left). The confidence level distribution for the best combination of hypothesis 2 (upper right). Pull distributions of photon energy and direction with superimposed fit to normal distribution (lower row). The fitted widths are close to the expected value.

Figure 6: Distributions of measured masses for the 7,434 events which pass the kinematic fit hypotheses. The  $\pi^0$  signal is slightly asymmetric but appears at the nominal value (upper left). No  $\eta$  background is present (upper right). The missing mass spectrum gives a slightly higher mass for the  $K_L$  (lower left), whereas the invariant  $\pi^0\pi^0$  mass spectrum gives a lower  $K_S$  mass.



# 3 Monte Carlo Studies

The reconstruction efficiency for the  $K_LK_S\pi^0\pi^0$  channel was determined with the CBGEANT [15] program package. It is a well known fact, that GEANT [4] does not simulate properly the interaction of low energy  $K_L$  mesons in matter. Therefore the  $K_L$  was represented by a geantino, a particle which does not interact at all. A total number of 20,000 events of the type  $K_L^{geantino}K_S\pi^0\pi^0$  were generated and subjected to the same selection cuts as described in the previous chapters. 2,689 events pass all cuts which gives a reconstruction efficiency of  $(13.4\pm0.3)\%$ . The number of events rejected by the cuts is detailed in Table 6.

It was estimated from the data, that about 10% of the  $K_S$  mesons were reconstructed with the wrong pion(see Fig 7). This was verified by the Monte Carlo data and is shown in Fig 9. It shows the same structure of wrong  $K_S$  combinations which amount to about 10%. The wrong combinations were the source of an enhancement in the  $K_S\pi^0$  invariant mass spectrum just below the  $K^*$  (see Fig. 8). This enhancement is also present in the Monte Carlo data set and disappears when wrongly combined  $K_S$  mesons are excluded. Once more the Monte Carlo data show the same behaviour as the real data and confirm the previous conclusions about the differences in the  $K_S$  and  $K_L$  spectra.

cuts	events
Monte Carlo events generated	20,000
all neutral events	18,348
8 PEDs	10,010
$970{ m MeV} < E_{tot} < 1450{ m MeV}$	9,916
no PED in crystal type 13	$7,\!827$
$  21^{circ} <  heta_{ec{p}} < 159^{circ}  $	$7,\!365$
$ m = 100  MeV/c^2 < m_{miss} < 600  MeV/c^2$	$6,\!646$
$\mathrm{CL}(\mathrm{K_L}8\gamma)>1\%$	$6,\!298$
$\mathrm{CL}(\mathrm{K_L}\mathrm{K_S}\pi^0\pi^0) > 1\%$	$4,\!096$
$  \mathrm{CL}(\mathrm{K_L} \mathrm{K_S} \pi^0 \pi^0) > 1\% \;  ext{and} \; \mathrm{CL}(\mathrm{K_L} \mathrm{K_S} \pi^0 \eta) < 1\%$	3,908
${ m CL}({ m K_L}{ m K_S}\pi^0\pi^0)>10\% \ \ { m and} \ \ { m CL}({ m K_L}{ m K_S}\pi^0\eta)<1\%$	$2,\!689$

Table 6: Number of Monte Carlo events rejected by cuts.

Figure 9: a) Invariant mass spectrum for  $\pi^0\pi^0$  combinations rejected by the kinematic fit. The background due to misidentified  $K_S$  corresponds to about 10%; b) Invariant  $K_S\pi^0$  and  $K_L\pi^0$  mass spectra. The  $K_S\pi^0$  spectrum shows an enhancement above the  $K_L\pi^0$  spectrum for masses between 700 and 800 MeV/c².

# 4 Partial Wave Analysis

The general features of  $K_LK_S\pi^0\pi^0$  final state are displayed in Fig. 10, where a clear  $\phi$  signal can be seen in the invariant  $K_LK_S$  mass spectrum as well as two strong  $K^*(892)$  bands in the  $m^2(K_L\pi^0)$  versus  $m^2(K_S\pi^0)$  scatter plot. Already at this initial step of the analysis the 2-body  $K^*K^*$  and the 3-body  $\phi\pi^0\pi^0$  final states are clearly visible. Almost every event contains one  $K^*$  and if this is treated as a stable particle the 4-body final state can be reduced to the 3-body final state  $K^*K\pi^0$  which could be suited for a Dalitz plot analysis, treating the  $K^*$  as a narrow particle. Events containing a  $K^*$  are selected by a simple mass cut and the Dalitz plot for the  $K^*K\pi^0$  final state is shown in Fig. 11. Two main features can be seen, a strong second horizontal  $K^*$  band and perhaps a vertical band at a  $K^*K$  invariant mass around  $1.4 \, \text{GeV}/\text{c}^2$ . If this band came from a particle, decaying to  $K^*K$ , its charge conjugation quantum number would be C=-1 in the  $K_LK_S\pi^0$  final state and the isospin could be I=0 or 1. But this structure may very well be a reflection from higher K-resonances, which are certainly hidden in this final state.

#### 4.1 PWA Formalism

The partial wave analysis was performed in the full 5-dimensional space of kinematic variables. The helicity formalism [5] was used for a description of the angular dependence of the amplitudes, which were restricted to be two-particle states. In terms of the isobar model [6], the initial  $\bar{p}p$  system is assumed to decay to the  $K_L K_S \pi^0 \pi^0$  final state through a series of quasi two-body decays. In the helicity formalism, an isobar of spin J decays into two daughters of spin  $S_1$  and  $S_2$ . They have total spin S and relative angular momentum L. The spin dependence of the transition can be written as a matrix [7]:

$$\mathcal{A}(J;LS) = \mathcal{D}_{\lambda.m}^J( heta,\phi) \cdot \langle J\lambda \mid LS0\lambda 
angle \langle S\lambda \mid S_1S_2\lambda_1, -\lambda_2 
angle imes F_L(q) imes \mathcal{BW}_L(m).$$

The matrix has  $(2S_1 + 1)(2S_2 + 1)$  rows and (2J + 1) columns. The row index  $\lambda = \lambda_1 - \lambda_2$  runs over all possible final state helicities, while the column index m runs over the magnetic sub-states of the isobar. In the rest frame of the isobar, q is the final state momentum, while  $\theta$  and  $\phi$  refer to the decay angles. The final amplitude (or weight for the current event) is obtained by taking the trace of the transition matrix and multiplying this number by eventual phase space and acceptance correction weights.  $F_L$  is the damping factor, and  $\mathcal{BW}_L$  is the Breit-Wigner amplitude for the isobar decay. The damping (or penetration) factors  $F_L(q)$  are given by [10]

$$F_0(q) = 1$$
 $F_1(q) = \sqrt{\frac{2z}{z+1}}$ 

$$F_2(q) \;\; = \;\; \sqrt{rac{13z^2}{(z-3)^2+9z}}$$

where  $z = (q[\text{MeV/c}]/197.3)^2$ . The Breit-Wigner factors are given by

$$\mathcal{BW}_L(m) = rac{m_0\Gamma_0}{m_0^2 - m^2 - im_0\Gamma(m)}$$

where

$$\Gamma(m)=\Gamma_0rac{m_0}{m}rac{q}{q_0}rac{F_L^2(q)}{F_L^2(q_0)}$$

with  $m_0$  and  $\Gamma_0$  the nominal mass and width of a resonance and  $q_0$  the corresponding decay momentum. For a state with nominal mass below the sum of the masses of its decay products, the daughter momentum  $q_0$  becomes imaginary. This problem was avoided by using the an energy independent width in the denominator of the Breit-Wigner function  $\mathcal{BW}_L(m)$ 

## 4.2 The $\pi\pi$ S-wave

For the  $\pi\pi$  S-wave, the K1 parametrization from Au et al. [9] is used in terms of S-wave phase shift  $\delta$  and inelasticity  $\eta$  in  $\pi\pi$  elastic scattering. The Breit-Wigner function  $\mathcal{BW}_L(m)$  is replaced by

$$\mathcal{T}_{elastic}(m_{\pi\pi}) = rac{m_{\pi\pi}}{q} \cdot rac{\eta \cdot e^{2i\delta} - 1}{2i},$$

where  $m_{\pi\pi}$  is the invariant mass of the  $2\pi^0$  and q is the breakup momentum of the pions in the  $\pi\pi$  rest frame,  $q = \sqrt{0.25 m_{\pi\pi} m_{\pi\pi} - m_{\pi}}$ . The amplitude is shown in Fig 12.

#### 4.3 The $K\pi$ S-wave

The  $K\pi$  S-wave amplitude and phase was measured by the LASS experiment [2] in the  $(K\pi)$ -mass range between 800 and 1600 MeV/c<sup>2</sup>. Their data are reproduced in Fig. 13 together with a fit, where the amplitude T is expressed in terms of the K matrix.

$$T(m_{\mathrm{K}\pi}) = rac{K}{1-iK},$$

The K matrix is written as  $K=\rho\hat{K}$ , where  $\rho=\frac{2q}{m_{K\pi}}$  and q is the decay momentum of the  $(K\pi)$ -system in its rest frame,  $q^2[m_{K\pi}^2-(m_K+m_\pi)^2][m_{K\pi}^2-(m_K-m_\pi)^2]/4m_{K\pi}^2$ . The  $\hat{K}$  parametrization [11] contains two terms, a pole term for the  $K_0^*(1430)$  and a background term:

$$\hat{K} = rac{m_0 \Gamma_0 / 
ho_0}{m_0^2 - m^2} + \hat{K}_{BG}.$$

The background term is parametrized in the effective range approximation

$$q\cot\delta=rac{1}{a}+rac{1}{2}bq^2,$$

where a is the scattering length and b the effective range. The phase  $\delta$  is related to the K matrix,  $K = 1/\cot \delta$ , which leads to the following expression for the background term in  $\hat{K}$ :

$$\hat{K}_{BG}=rac{am_{ ext{K}\pi}}{2+abq^2}.$$

The free parameters a and b are determined by a fit of T to the LASS data, Fig. 13. The mass  $(m_o)$  and width  $(\Gamma_o)$  are fixed to the values found by S.v. Dombrowski in his fits to the same data and  $q_o$  has the value  $q_o = 0.57149$ . For the two remaining free parameters I find the values  $a = (1.79 \pm 0.09) GeV^{-1}$  and  $b = (3.46 \pm 0.2) GeV^{-1}$  in the fit to the absolute value of the amplitude. The fit to the phase gives slightly different parameters. The  $K\pi$  S-wave amplitude which will finally be used in the partial-wave analysis is given by

$$\mathcal{T} = rac{m_{\mathrm{K}\pi}}{q} \cdot T$$

and is shown in Fig 14.

Figure 10: The  $K_LK_S\pi^0\pi^0$  final state has a  $\phi$  and a  $K^*$  component; a) the  $K_LK_S$  invariant mass distribution and b) the  $K\pi^0$  scatter plot.

Figure 11: The  $K^*K\pi^0$  Dalitz plot.

Figure 12: The Au et al.  $\pi\pi$  S-wave as used in the partial-wave analysis program. The upper left figure shows the absolute value of  $\mathcal{T}$ , the upper right one shows the real part of  $\mathcal{T}$ , the lower left one shows the imaginary part of  $\mathcal{T}$  and the lower right graph gives the Argand diagram.

Figure 13: Data from the LASS experiment for the magnitude and phase of the  $I=\frac{1}{2}$  K $\pi$  S-wave amplitude in the mass region below 1.6 GeV/c². The curves show the result of the fit described in the text.

Figure 14: The  $K\pi$  S-wave as used in the partial-wave analysis program. The upper left figure shows the absolute value of  $\mathcal{T}$ , the upper right one shows the real part of  $\mathcal{T}$ , the lower left one shows the imaginary part of  $\mathcal{T}$  and the lower right graph gives the Argand diagram.

## 5 PWA Fits

The five dimensional space of kinematic variables is taken into account by an unbinned maximum likelihood fit of the partial-wave amplitudes to the experimental data. The program package MAXTOOL was developed for that purpose by C. Felix. It incorporates a slightly modified version of the SPIN program [7] and the standard CERN minimization package MINUIT [12].

The quantum numbers of the initial  $\bar{p}p$  state are restricted by parity and C-parity conservation. The annihilation into the  $K_LK_S\pi^0\pi^0$  final state can only occur from the  ${}^3S_1$  ( $J^{PC}=1^{--}$ ) or the  ${}^1P_1$  ( $J^{PC}=1^{+-}$ )  $\bar{p}p$  atomic orbitals. Annihilation from the S-wave only will be described first before P-wave annihilation will be allowed in the fits.

# 5.1 Annihilation from pp S-wave

It was shown above (Fig. 10) that the  $K_LK_S\pi^0\pi^0$  final state contains many  $K^*$  and some  $\phi$  mesons. The simplest fit therefore contains the following amplitudes. The following fits have names attached, given in parentheses, like (huntk1). These names have no meaning, they are just file names and are given for bookkeeping purposes.

#### Fit 1 amplitudes: (huntk1)

- 1.  $\bar{p}p(1^{--}) \to (K\pi)_S K^*(892), L = 0, S = 1$ The  $(K\pi)S$ -wave comes from LASS data and was described above. It is in a relative S-wave (L = 0) with the  $K^*$  and the total spin S is given by that of the  $K^*$ , S = 1. The  $(K\pi)S$ -wave disintegrates into a K and a  $\pi^0$  with L = 0, and the  $K^*$  meson decays to  $K_L\pi^0$  and  $K_S\pi^0$  with relative angular momentum L = 1. The letters L and S describe the relative angular momentum of two decay products and their total spin.
- 2.  $\bar{p}p(1^{--}) \to K^*(892)\bar{K}^*(892)$ , L=1, S=0, 2The two  $K^*$  are in a relative P-wave and their spins add up to S=0 and S=2. The  $K^*$ 's decay as above.
- 3.  $\bar{p}p(1^{--}) \rightarrow \phi(\pi\pi)_S$ , L=0, S=1The  $\phi$  decays to  $K_LK_S$  with angular momentum L=1 and the  $(\pi\pi)S$ -wave decays to two pions with, obviously, L=0.
- 4.  $\bar{p}p(1^{--}) \to K_1(m)K^0$  L=0, S=1The mass of the  $K_1(m)$  is varied in the range 1100 to 1700 MeV/c² where for each mass interval a new fit is made. The width of this hypothetical  $K_1(m)$  is fixed at 150 MeV/c². For the  $K_1(m)$  decay four different modes

 $egin{array}{lll} {
m are \ considered:} & {
m K}_1(m) & 
ightarrow & {
m K}^*(892)\pi, & L=0, S=1 \ {
m K}_1(m) & 
ightarrow & {
m K}^*(892)\pi, & L=2, S=1 \ {
m K}_1(m) & 
ightarrow & ({
m K}\pi)_{
m S}\pi, & L=1, S=0 \ {
m K}_1(m) & 
ightarrow & {
m K}^0(\pi\pi)_{
m S}, & L=1, S=0 \ \end{array}$ 

#### 5. Incoherent background amplitude.

The result of this fit is shown in Figs. 1516 and Table 7 and it gives already a fairly good description of the data. The aim of this first fit was, however, to identify higher K-resonances which might contribute to the  $K_LK_S\pi^0\pi^0$  final state. These states might be indicated in the log likelihood versus mass plot of Fig. 16, which shows a broad shoulder between 1200 and 1300 MeV/c<sup>2</sup> and a clear peak just above 1400 MeV/c<sup>2</sup>. This is even more obvious in the  $\langle \chi^2 \rangle$ -plot, which shows two distinct minima at those masses. These structures are probably the well known strange resonances  $K_1(1270)$  and  $K_1(1400)$  which will be included in the following fits with their PDG masses and widths.

Fit 2 amplitudes: (basicfit) The first three amplitudes and the incoherent background are the same as in fit 1 and the  $K_1(m)$  is replaced by  $K_1(1270)$  and  $K_1(1400)$  with the same four decay modes as in fit 1.

The result of this fit is shown in Fig. 17 and Table 8. and it gives a good description of the data, except for the  $K_LK_S\pi^0$  spectrum, where the sharp rise around  $1400\,\mathrm{MeV/c^2}$  is not well reproduced. As can be seen in Table 8, some of the  $K_1$  amplitudes have rather low intensities and an arbitrary minimum intensity of 1% will be required for the amplitude to be introduced in the following fits. This leads to the Fit 3 amplitudes, which is the basic fit of this analysis, including only amplitudes for well established particles.

Fit 3 amplitudes: (vb-g0) Although already given in the first two fits in different combinations, the amplitudes for fit 3, the basic amplitudes of this analysis, are repeated here, since the following fits, which include new, or not well known particles, will be compared with this fit.

1. 
$$\bar{p}p(1^{--}) \rightarrow (K\pi)_S K^*(892), L = 0, S = 1$$
  
 $(K\pi)_S \rightarrow K\pi, L = 0, S = 0$   
 $K^*(892) \rightarrow K\pi, L = 1, S = 1$ 

2. 
$$\bar{p}p(1^{--}) \to K^*(892)\bar{K}^*(892), L = 1, S = 0$$
  
 $K^*(892) \to K\pi, L = 1, S = 1$ 

3. 
$$\bar{\mathbf{p}}\mathbf{p}(1^{--}) \to \mathbf{K}^*(892)\bar{\mathbf{K}}^*(892), \ L=1, S=2$$
  
  $\mathbf{K}^*(892) \to \mathbf{K}\pi, \ L=1, S=1$ 

4. 
$$\bar{p}p(1^{--}) \rightarrow K_1(1270)K^0, \ L = 0, S = 1$$
  
 $K_1(1270) \rightarrow K^*(892)\pi, \ L = 0, S = 1$   
 $K^*(892) \rightarrow K\pi, \ L = 1, S = 1$ 

5. 
$$\bar{p}p(1^{--}) \rightarrow K_1(1400)K^0, L = 0, S = 1$$
  
 $K_1(1400) \rightarrow K^*(892)\pi, L = 0, S = 1$   
 $K^*(892) \rightarrow K\pi, L = 1, S = 1$ 

7. 
$$\bar{\mathrm{p}}\mathrm{p}(1^{--}) \to \mathrm{K}_1(1400)\mathrm{K}^0, \ L=0, S=1 \ \mathrm{K}_1(1400) \to (\mathrm{K}\pi)_\mathrm{S}\pi, \ L=1, S=0 \ (\mathrm{K}\pi)_\mathrm{S} \to \mathrm{K}\pi, \ L=0, S=0$$

8. 
$$\bar{p}p(1^{--}) \to \phi(\pi\pi)_{S}, L = 0, S = 1$$
  
 $\phi \to K_{L}K_{S}, L = 0, S = 1$ 

9. Incoherent background amplitude.

This fit contains 16 free parameters, 9 intensities and 7 phases. The invariant mass distributions for this fit are not shown, since they are almost identical to fit 2, shown in Fig. 17. The numerical results are given in Table 9.

The quality of the fits will be judged by two numbers, the log likelihood of the fit, and the average  $\chi^2$  value of the five, one-dimensional invariant mass distributions  $m(\pi^0\pi^0)$ ,  $m(\pi^0\mathrm{K}^0)$ ,  $m(\mathrm{K_LK_S})$ ,  $m(\pi^0\pi^0\mathrm{K}^0)$ ,  $m(\pi^0\mathrm{K_LK_S})$ . This fit gives the benchmark values,  $\log\mathcal{L}=3074$  and  $\langle\chi^2\rangle=1.9$ . A technical point should be mentioned here which concerns the fits searching for new particles  $\mathrm{X}(J^{PC})$ . A mass scan is made in those fits and for reasons of computing time, the phases of the amplitudes of the basic fit are fixed. This results in slightly lower benchmark values for the quality numbers, namely  $\log\mathcal{L}=3031$  and  $\langle\chi^2\rangle=2.2$ .

Fit 4 amplitudes: (hunto-kstarpi) Search for  $X(0^-) \to K^*\pi$  contributions, like K(1460), in the mass range from 1350 to 1750 MeV/c², with width  $\Gamma = 260 \text{ MeV/c²}$ . The likelihood and  $\langle \chi^2 \rangle$  stay practically constant over the whole mass range,  $\log \mathcal{L} = 2990 \pm 0.5$  and  $\langle \chi^2 \rangle = 2.51 \pm 0.1$ , and the maximum contribution is 0.2%. If the K(1460) is added with the PDG values to the basic amplitudes (vb-k1460k), it is rejected by the fit. The conclusion is that no  $X(0^-) \to K^*\pi$  is needed to fit the data.

Fit 5 amplitudes: (hunt1-kstarpi) Search for  $X(1^-) \to K^*\pi$  contributions, like  $K^*(1410)$ , in the mass range 1200 to 1600 MeV/c<sup>2</sup>, with  $\Gamma = 227 \,\text{MeV/c}^2$ . The likelihood in constantly rising, from 3031 to 3041, over the scanned mass

range, and a maximum intensity of 0.3% is allowed. If the  $K^*(1410)$  is added with the PDG values to the *basic amplitudes* (vb-kstar1410k), it is rejected by the fit. The conclusion is that no  $X(1^-) \to K^*\pi$  is needed to fit the data.

Fit 6 amplitudes: (hunt2+kstarpi) Search for  $X(2^+) \to K^*\pi$  contributions, like  $K_2^*(1430)$ , in the mass range 1200 to 1600 MeV/c², with  $\Gamma = 109 \, \text{MeV/c²}$ . Around 1400 MeV/c² log  $\mathcal{L}$  rises to 3050 and  $\langle \chi^2 \rangle$  reaches a minimum, indicating perhaps a weak production of  $K_2^*(1430)$  with an intensity of 0.6%. But there is also a local maximum, resp. minimum between 1200 and 1300 MeV/c². Perhaps these two bumps are due to  $K_1(1270)$  and  $K_1(1400)$ , indicating that the fit cannot distinguish between  $J^{PC}$ =1<sup>+</sup> and 2<sup>+</sup>. If the  $K_2^*(1430)$  is added with the PDG values to the basic amplitudes (vb-k2star1430k), it does not take away any intensity from  $K_1(1270)$  or  $K_1(1400)$  and is rejected by the fit. The conclusion is that no  $X(2^+) \to K^*\pi$  is needed to fit the data.

Fit 7 amplitudes: (hunt2-kstark) Search for  $X(2^{--}) \to K^*K$  contributions, like the missing D-wave mesons, expected around  $1.7\,\mathrm{GeV/c^2}$ . The mass range scanned was from 1350 to  $1750\,\mathrm{MeV/c^2}$ . There is a nice, but small maximum in  $\log\mathcal{L}$  around a mass of  $1600\,\mathrm{MeV/c^2}$ , accompanied by a minimum in  $\langle\chi^2\rangle$  around  $1550\,\mathrm{MeV/c^2}$ . The increase in likelihood is about  $\Delta\log\mathcal{L}=15$  and the intensity is 0.3%. Perhaps this is a hint for the missing  $2^{--}$  state, but too weak to be considered further. The conclusion is that no  $X(2^{--}) \to K^*K$  is needed to fit the data.

Fit 8 amplitudes: (hunt1-phi1680) Search for  $X(1^{--}) \to K^*K$  contributions, like  $\phi(1680)$ , in the mass range 1350 to 1750 MeV/c², with  $\Gamma=150\,\mathrm{MeV/c^2}$ . The mass scan shows two clear maxima, one around  $1400\,\mathrm{MeV/c^2}$  and one below  $1700\,\mathrm{MeV/c^2}$  and an intensity just over 1%. The higher mass maximum might indicate a contribution of the  $\phi(1680)$ . If it is added with the PDG values to the basic amplitudes (vb-phi1680pi), the fit improves slightly,  $\log\mathcal{L}=3103$  and  $\langle\chi^2\rangle=1.9$  and the intensity is 1.4%. The  $\phi(1680)$  might be weakly present in the  $K_LK_S\pi^0\pi^0$  final state.

To get more information about the first maximum in  $\log \mathcal{L}$ , a finer mass and width scan (hunt1-kstark, hunt-rho1400width) is done in the range 1200 to  $1600\,\mathrm{MeV/c^2}$  and  $100\,\mathrm{to}\,400\,\mathrm{MeV/c^2}$ . The fit with the highest probability gives a mass of  $1380\,\mathrm{MeV/c^2}$  and a not well determined width with equal probability between 200 and  $400\,\mathrm{MeV/c^2}$ . Nevertheless, a  $1^{--}$  amplitude with  $m=1380\,\mathrm{MeV/c^2}$  and  $\Gamma=300\,\mathrm{MeV/c^2}$  was added to the basic amplitudes (vb-rho1400pi). The fit has the same quality as the above one with  $\phi(1680)$ ,  $\log \mathcal{L}=3103$  and  $\langle \chi^2 \rangle = 1.8$ , and the amplitude contributes 1.1%. Could this be a new particle, the  $\phi(1380)$ , or does the undetermined width just indicate a background amplitude?

Fit 9 amplitudes: (hunt1-phipi) Search for  $X(1^{--}) \to \phi \pi$  contributions, like  $b_1(1235)$  or  $\rho(1450)$ , in the mass range 1200 to 1700 MeV/c², with  $\Gamma = 150 \text{ MeV/c²}$ . There is a nice maximum around 1500 MeV/c² which has a  $\Delta \log \mathcal{L} = 15$  and an intensity of 0.6%. Is this the GAMS krypto-exotic C(1480)? If it is added with their values, m = 1480 MeV/c² and  $\Gamma = 130 \text{ MeV/c²}$ , to the basic amplitudes (vb-c1480pi), the fit does not improve,  $\log \mathcal{L} = 3077$  and  $\langle \chi^2 \rangle = 1.9$  and the intensity is small, 0.4%. The  $\phi \pi$  signal will be further investigated with different methods in a forthcoming technical report on the reaction  $\bar{p}p \to \phi \pi^0 \pi^0$ . The conclusion here is, however, that  $X(1^{--}) \to \phi \pi$  is not needed to fit the data.

The  $b_1(1235) \to \phi \pi$  was also added to the fit (vb-b1235pi) with its PDG values. The likelihood did not improve and the intensity was 0.03%, i.e. practically zero. It will not be considered further.

Fit 10 amplitudes: (hunt1+-kstark) Search for  $X(1^{+-}) \to K^*K$  contributions, like  $h'_1(1380)$ , in the mass range 1350 to 1650 MeV/c<sup>2</sup>, with  $\Gamma = 223$  MeV/c<sup>2</sup>. Similar to the search in fit 8, here are also two maxima in the  $\log \mathcal{L}$ , one at  $m=1380\,{
m MeV/c^2}$  and one near  $m=1500\,{
m MeV/c^2}$ , but the  $\langle\chi^2\rangle$  versus mass plot shows only one minimum below  $1400\,\mathrm{MeV/c^2}$ . The search for the decay  $\mathrm{X}(1^{+-})$  $\rightarrow (K\pi)_s K$  (hunt1+-kpisk) shows only one broad bump, resp. minimum, between 1450 and 1650 MeV/c<sup>2</sup>, but with very small intensity of 0.8\%, which might indicate that the peak at 1380 MeV/c<sup>2</sup> is an artifact of the K\*K threshold. The  $(K\pi)_s K$  will not be included in later fits. The 1<sup>+-</sup> amplitude gives with 2.7% the highest contribution of all the particles searched for so far. This is perhaps the LASS h<sub>1</sub>(1380), which is added with the PDG values to the basic amplitudes (vbh1380). The fit improves significantly,  $\log \mathcal{L} = 3116$  and  $\langle \chi^2 \rangle = 1.7$  and the intensity is 8%. But it seems very strange that also the incoherent background contribution rises from 12\% to 18\%. But the 1<sup>+-</sup>amplitude is definitely needed and a systematic mass and width scan is made, to find its parameters. The corresponding likelihood and  $\langle \chi^2 \rangle$  plots as a function of the width are shown in Fig 18

- 1.  $m(1^{+-})=1390\,{
  m MeV/c^2}$ , width scan from 50 to  $250\,{
  m MeV/c^2}$ . The likelihood reaches a maximum around  $150\,{
  m MeV/c^2}$ ,  $\log\mathcal{L}\approx3070$ , and then stays flat around that value. The same is true for the minimum in  $\langle\chi^2\rangle\approx1.97$ .
- 2.  $m(1^{+-}) = 1420 \, \mathrm{MeV/c^2}$ , width scan from 100 to  $400 \, \mathrm{MeV/c^2}$ . The likelihood is constantly rising over the whole range and reaches  $\log \mathcal{L} \approx 3177$  for  $400 \, \mathrm{MeV/c^2}$  width. The  $\langle \chi^2 \rangle$  behaviour is different and has a minimum,  $\langle \chi^2 \rangle \approx 1.67$ , between 150 and 200  $\, \mathrm{MeV/c^2}$ .
- 3.  $m(1^{+-}) = 1440 \,\mathrm{MeV/c^2}$ , width scan from 100 to  $400 \,\mathrm{MeV/c^2}$ . The likelihood is again constantly rising over the whole range and reaches

the same maximum as in the previous scan. The  $\langle \chi^2 \rangle$  behaviour is again different and has a minimum,  $\langle \chi^2 \rangle \approx 1.68$ , between 150 and 250 MeV/c<sup>2</sup>.

- 4.  $m(1^{+-}) = 1460 \, \mathrm{MeV/c^2}$ , width scan from 100 to  $400 \, \mathrm{MeV/c^2}$ . The likelihood is again constantly rising over the whole range and reaches the same maximum as in the previous scan. The  $\langle \chi^2 \rangle$  behaviour is again different and has a minimum,  $\langle \chi^2 \rangle \approx 1.7$ , between 150 and 250 MeV/c<sup>2</sup>.
- 5.  $m(1^{+-}) = 1480 \,\mathrm{MeV/c^2}$ , width scan from 100 to  $300 \,\mathrm{MeV/c^2}$ . This time the likelihood reaches a nice maximum,  $\log \mathcal{L} \approx 3145$  around  $150 \,\mathrm{MeV/c^2}$ , with a corresponding minimum at  $\langle \chi^2 \rangle \approx 1.75$ .

Unfortunately, the likelihood versus width plots of the best fits do not exhibit a clear peak for the best width in the scanned range. Therefore, another scan was made for a mass of  $m(1^{+-})=1430\,\mathrm{MeV/c^2}$  where the width was varied in a wider range, between 200 and  $600\,\mathrm{MeV/c^2}$ . Now the likelihood peaks around  $400\,\mathrm{MeV/c^2}$ . There is no question, that a  $J^{PC}=1^{-+}$  state around  $1430\,\mathrm{MeV/c^2}$  is needed, but what is the width? Is it around  $200\,\mathrm{MeV/c^2}$ , as indicated by the  $\langle \chi^2 \rangle$  plots or is it around  $400\,\mathrm{MeV/c^2}$ , as indicated by the likelihood plots? The very large width might take care of some additional small amplitude and some background. I propose to use a width of  $250\,\mathrm{MeV/c^2}$ , closer to the value indicated by the  $\langle \chi^2 \rangle$ , with a large asymmetric error of  $+150\,\mathrm{MeV/c^2}$  and  $-100\,\mathrm{MeV/c^2}$ . A fit with these parameters (vb-h1430w250) is shown in Fig. 19 and the results are in Table 10. The projections are well described by this fit and, in particular, the sharp rise in the  $K_L K_S \pi^0$  spectrum around  $1400\,\mathrm{MeV/c^2}$  can be reproduced.

Fit 11 amplitudes: (vb-h1430+phi1680) The only other amplitudes, which had some contribution, were discussed in fit 8, a  $\phi(1380)$  and a  $\phi(1680)$  decaying to K\*K. These were added one by one to the amplitudes of fit 10.

- 1. Fit 10 amplitudes  $+ \bar{p}p \rightarrow \phi(1680)\pi$ This fit has a slightly higher likelihood than fit 10, but the same  $\langle \chi^2 \rangle$ ,  $\log \mathcal{L} = 3186$  and  $\langle \chi^2 \rangle = 1.68$ . The contribution of the  $\phi(1680)$  is negligible, only 0.4%.
- 2. Fit 10 amplitudes  $+ \bar{p}p \rightarrow \phi(1380)\pi$ This fit has even a lower likelihood than fit 10, and a slightly worse  $\langle \chi^2 \rangle$ ,  $\log \mathcal{L} = 3149$  and  $\langle \chi^2 \rangle = 1.8$ . The contribution of the  $\phi(1680)$  is low, only 0.8%.

The conclusion is that  $\phi(1380)$  and  $\phi(1680)$  are not needed to describe the data.

## 5.2 Annihilation from pp S- and P-wave

The same set of amplitudes are used for  $\bar{p}p$  annihilation from the  $^1P_1$  state with the adaption of angular momentum and spin assignments for the intermediate two-particle combinations. The final transition amplitude is an incoherent sum over the contributing initial states:

$$w = \{a \mid \mathcal{A}_{1--} \mid^2 + (1-a) \mid \mathcal{A}_{1+-} \mid^2\} \cdot w_{PS} ,$$

where  $\mathcal{A}_{1^{--}}$  is the coherent sum over all amplitudes from the  ${}^{3}S_{1}$  initial state,  $\mathcal{A}_{1^{+-}}$  is the coherent sum over all amplitudes from the  ${}^{1}P_{1}$  initial state and  $w_{PS}$  is the phase space weight.

The S- and P-wave fit corresponding fit 2 has a slightly better  $\log \mathcal{L}$ , it rises from 3092 to 3153, but the number of free parameters is almost twice as large as for the S-wave fit only. The main effect is that the inclusion of P-wave annihilation reduces the background contribution to 8%. The total P-wave contribution comes out to be almost 20%. Due to the only slight increase in  $\log \mathcal{L}$  in spite of the much larger number of free parameters, P-wave annihilation shall not be considered further.

#### 5.3 Conclusion

The reaction  $\bar{p}p \to K_L K_S \pi^0 \pi^0$  can be well described contributions from the two-body final states  $K^*K^*$ ,  $K_1(1270)$  K,  $K_1(1400)$  K,  $\phi(\pi^0\pi^0)_S$  and a new  $J^{PC}=1^{+-}$  state with mass and width  $m=1430\pm30~{\rm MeV/c^2}$ ,  $\Gamma=250^{+150}_{-100}~{\rm MeV/c^2}$ . The intensities and phases for the final fit with pure S-wave annihilation were already given in Table 10. The quality of the fit can be appreciated by looking at one dimensional projections of the invariant mass distributions in Fig. 19.

The  $K_1(1270)$  and  $K_1(1400)$  are mixtures of the pure SU(3) quark model states  $K_{1A}$  and  $K_{1B}$  and should be observed with roughly equal probability, which is clearly not the case. The dominance of  $K_1(1400)$  is simply a reflection of its preferred decay mode into  $K^*K$ , whereas the  $K_1(1270)$  prefers  $K\rho$ , which is not observed here.

The  $X(1^{+-})$  state which is needed for a satisfactory description of the  $K_LK_S\pi^0\pi^0$  final state could be the *strangeonium* of the axial vector nonet, the  $h_1(1380)$  as it is called by PDG. A candidate for this state was seen first in a partial wave analysis of the reaction  $K^-p \rightarrow K_SK^{\pm}\pi^{\mp}\Lambda$  [2]. The mass and width measured in this analysis is slightly larger:

$$m_{
m h_1'} = (1430 \pm 30) \, {
m MeV/c^2} ~~\Gamma = 250^{+150}_{-100} \, {
m MeV/c^2} ~.$$

Fit 1	$\log \mathcal{L} = 3023$			$\langle \chi^2  angle$	2.1	
Amplitude	Inte	ensit	y [%]	Phase [deg]		
$(K\pi)_S K^*$ S-wave	6	$\pm$ 16		0	fixed	ł
$K^*\bar{K}^*$ S-wave	7	$\pm$	9	320	$\pm$	11
$K^*\bar{K}^*$ D-wave	6	±	13	194	土	10
$\phi(\pi\pi)_{ m S}$ S-wave	4	±	6	201	±	11
$K_1(m)K$ S-wave total	54	$\pm$	58			
with contributions from						
$\mathrm{K}_{1}(m){ ightarrow}\mathrm{K}^{st}\pi^{0}$ S-wave	37	$\pm$	53	282	$\pm$	16
$\mathrm{K}_{1}(m){ ightarrow}\mathrm{K}^{st}\pi^{0}\mathrm{D ext{-}wave}$	5	$\pm$	7	219	$\pm$	6
$K_1(m){ ightarrow}(K\pi)_{ m S}\pi^0$ P-wave	10	$\pm$	22	232	$\pm$	7
$\mathrm{K}_{1}(m){ ightarrow}\mathrm{K}(\pi\pi)_{\mathrm{S}}$ P-wave	2	$\pm$	8	217	$\pm$	23
Incoherent background	23	±	100			

Table 7: Fit 1 amplitudes and phases.

Fit 2	$\log \mathcal{L} = 3092$			$\langle \chi^2 \rangle = 1.8$			
Amplitude	Inter	sity	[%]	Phase [deg]			
K*K* S-wave	3.5	$\pm$	0.3	(	0 fixed		
$K^*\bar{K}^*$ D-wave	4.8	土	0.6	232	±	2	
$K_1(1270) { ightarrow} K^*\pi^0$ S-wave	4.5	土	0.4	9	土	3	
$\mathrm{K}_{1}(1270){ ightarrow}\mathrm{K}^{*}\pi^{0}\;\mathrm{D ext{-}wave}$	0.04	$\pm$	0.1	249	$\pm$	$_{ m large}$	
$K_1(1270) \rightarrow (K\pi)_S \pi^0$ P-wave	1	±	0.5	166	土	8	
$K_1(1270){ ightarrow}K(\pi\pi)_{ m S}$ P-wave	1	±	1	191	土	21	
$K_1(1400) { ightarrow} K^*\pi^0$ S-wave	55	$\pm$	2	301	±	1	
$K_1(1400){ ightarrow} K^*\pi^0$ D-wave	1.6	±	0.4	258	±	3	
$K_1(1400){ ightarrow}(K\pi)_{ m S}\pi^0$ P-wave	3	$\pm$	2	253	<b>±</b>	7	
$K_1(1400){ ightarrow} K(\pi\pi)_{ m S}$ P-wave	0.2	±	2	184	±	$_{ m large}$	
$\phi(\pi\pi)_{ m S}$ S-wave	2.3	土	0.2	244	±	14	
$(K\pi)_SK^*$ S-wave	10	土	2	76	±	3	
Incoherent background	13	±	1				

Table 8: Fit 2 amplitudes and phases.

Fit 3	$\log \mathcal{L} = 3074$			$\langle \chi^{2}  angle = 1.9$		
Amplitude	Inte	nsity	7 [%]	Phase [deg]		
$(K\pi)_S K^*$ S-wave	10	±	3	0	fixed	ł
$K^*\bar{K}^*$ S-wave	3.1	$\pm$	0.4	257	$\pm$	9
$K^*\bar{K}^*$ D-wave	4.6	±	0.8	130	±	10
$\mathrm{K}_{1}(1270){ ightarrow}\mathrm{K}^{*}\pi^{0}\mathrm{S ext{-}wave}$	4.7	±	1	281	±	7
$\mathrm{K}_{1}(1400){ ightarrow}\mathrm{K}^{st}\pi^{0}$ S-wave	58	$\pm$	9	210	$\pm$	5
$\mathrm{K}_{1}(1400){ ightarrow}\mathrm{K}^{st}\pi^{0}\mathrm{D ext{-}wave}$	2.2	±	0.7	156	±	8
$K_1(1400) \rightarrow (K\pi)_S \pi^0$ P-wave	3.2	±	0.5	176	±	7
$\phi(\pi\pi)_{ m S}$ S-wave	2.2	土	0.3	139	土	11
Incoherent background	12	±	2			

Table 9: Fit 3 amplitudes and phases.

Fit 10 final	$\log \mathcal{L} = 3172$			$\langle \chi$	1.7	
Amplitude	Inter	$_{ m isity}$	[%]	Phase [deg]		
$(K\pi)_{\mathrm{S}}K^{*}$ S-wave	10.7	±	6	(	ed	
K*K* S-wave	3.3	±	1	166	±	7
$K^*\bar{K}^*$ D-wave	2.4	±	0.4	18	±	11
$K_1(1270) { ightarrow} K^*\pi^0$ S-wave	3.8	±	1	134	±	9
$K_1(1400){ ightarrow} K^*\pi^0$ S-wave	52.7	±	3	74	±	6
$K_1(1400){ ightarrow} K^*\pi^0$ D-wave	0.3	$\pm$	2	73	$\pm$	$_{ m large}$
$K_1(1400) \rightarrow (K\pi)_S \pi^0$ P-wave	1.9	±	1	39	±	10
$\phi(\pi\pi)_{ m S}$ S-wave	1.7	±	1	6	±	15
$X(1^{+-}) \rightarrow K^*K$ S-wave	13.4	<b>±</b>	1	2	土	9
M(1 ) THE HOWAVE	- •					

Table 10: Amplitudes and phases for the final fit.

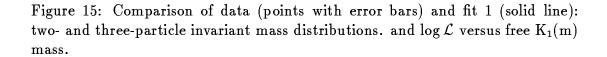
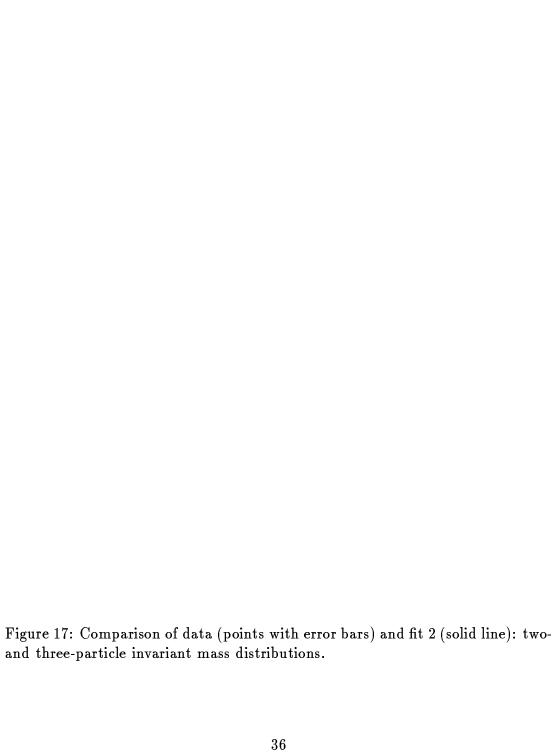


Figure 16: Fit quality versus  $K_1(m)$  mass. The left figure shows the log likelihood value and the right figure the average  $\chi^2$  as a function of  $K_1$  mass. Structures corresponding to  $K_1(1270)$  and  $K_1(1400)$  can be seen clearly.



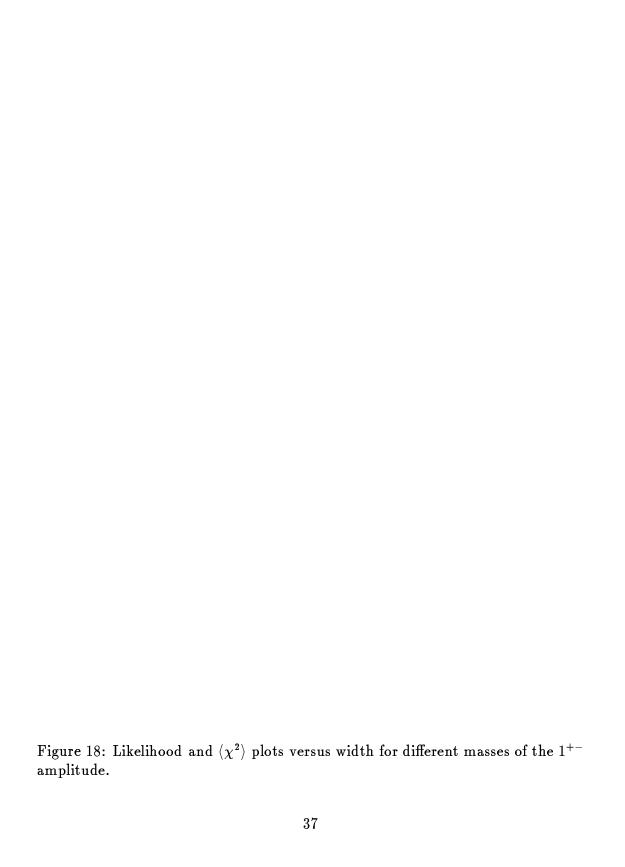


Figure 19: Comparison of data (points with error bars) and fit (solid line). The amplitudes are as in Fit 3 plus an amplitude for the reaction:  $\bar{p}p \rightarrow X(1430, 1^{+-})\pi$ ,  $X \rightarrow K^*K$ . Two- and three-particle invariant mass distributions.

# References

- [1] S. I. Bityukov et al., Phys. Lett.B188(1987)383.
- [2] D. Aston, Phys. Lett.B201(1988)573.
- [3] E. Aker et al., Nucl. Instr. Methods A 321 (1992) 69.
- [4] R. Brun et al., GEANT3, Internal Report CERN DD/EE/84-1 (1986).
- [5] M. Jacob and G. C. Wick, Ann. Phys. (N.Y.)7(1959)404.
- [6] D. Meindon et al., Phys. Rev.D11(1975)3165
- [7] C. Amsler and J. C. Bizot, Comp. Phys. Comm. 30(1983)21.
- [8] C. Amsler et al., Phys. Lett.B311(1993)362.
- [9] K. L. Au et al., Phys. Rev. D35(1987)1633.
- [10] F. von Hippel and C. Quigg, Phys. Rev. D5(1972)624.
- [11] S. von Dombrowski, private communication.
- [12] CERN Program Library Entry D506, MINUIT, Version 92.1 (1992).
- [13] J. H. Friedman, Phys. Rev. D9(1974)3053.
- [14] Review of Particle Properties, Phys. Rev. D45(1992).
- [15] R. Bossingham, Monte Carlo Software CBGEANT, Ver. 4.06/03, CB-note 169 (1992).